Originalarbeit

Berg Huettenmaenn Monatsh (2025) Vol. 170 (7): 393–398
https://doi.org/10.1007/s00501-025-01596-3

BHM Berg- und Hüttenmännische Monatshefte

Towards a Better Understanding of ARA Conversion

Thomas Nanz[1,2], Matthias Kiss[1,2], Golnaz Zarabian[1], Barbara Weiß[1,2], Markus Bösenhofer[1], Christine Gruber[2], Johannes Rieger[2], Christoph Feilmayr[3], Hugo Stocker[4], and Michael Harasek[1]

[1]Institute of Chemical, Environmental and Bioscience Engineering, Technische Universität Wien, Vienna, Austria
[2]K1-MET GmbH, Linz, Austria
[3]voestalpine Stahl GmbH, Linz, Austria
[4]voestalpine Stahl Donawitz GmbH, Leoben, Austria

Received March 28, 2025; accepted April 8, 2025; published online May 9, 2025

Abstract: To better understand the conversion of alternative reducing agents (ARAs) in the blast furnace, a test reactor, designed to resemble blast furnace conditions, was built. A corresponding CFD model of the reactor was developed to enhance the understanding of the flow field, heat transfer, and reactions inside the reactor during ARA conversion. The temperatures inside the reactor, the calculated residence time of the particles, and the calculated burnout suggest a good agreement of the simulation and the experiment. The presented approach allows testing ARAs for the applicability in the blast furnace.

Keywords: Alternative reducing agents (ARA), Blast furnace, CFD simulation, Test reactor, Pulverized coal injection

Hin zu einem besseren Verständnis der ARA-Konversion

Zusammenfassung: Für ein besseres Verständnis der Konversion von alternativen Reduktionsmitteln (ARAs) im Hochofen wurde ein Testreaktor entwickelt, der die Bedingungen im Hochofen nachahmt. Ein CFD-Model des Reaktors wurde entwickelt, um das Verständnis des Strömungsfeldes, des Wärmeübergangs und der Reaktionen im Reaktor während der ARA-Konversion zu erweitern. Die Temperaturen im Reaktor, die berechnete Verweilzeit der Partikel und der berechnete Ausbrand deuten auf eine gute Übereinstimmung zwischen der Simulation und dem Experiment hin. Der vorgestellte Ansatz ermöglicht das Testen von ARAs auf ihre Anwendbarkeit im Hochofen.

Schlüsselwörter: Alternative Reduktionsmittel (ARA), Hochofen, CFD-Simulation, Testreaktor, Konversion von pulverisiertem Kohlenstoff

T. Nanz (✉)
Institute of Chemical, Environmental and Bioscience Engineering,
Technische Universität Wien,
Getreidemarkt 9,
1060 Vienna, Austria
thomas.nanz@tuwien.ac.at

1. Introduction

The use of alternative reducing agents (ARAs) in the blast furnace (BF), such as pulverized coal (PC) and biochar, gains increased attention in the pursuit of improving efficiency of the direct injection and reducing CO_2 emissions [1]. The injection of ARAs into the BF raceway zone can partially substitute metallurgical coke in the iron-making process. Understanding the conversion of ARAs is of vital importance to evaluate their applicability in the BF. Reliable knowledge of conversion rates and kinetic parameters is critical to identifying suitable ARAs. The harsh conditions in the raceway zone make direct measurements impossible. A unique ARA reactor (test reactor) was developed in collaboration between voestalpine Stahl, voestalpine Stahl Donawitz, K1-MET, and Technische Universität Wien (Institute of Chemical, Environmental and Bioscience Engineering) to improve the understanding of thermochemical coal conversion and analyze alternative solid fuels, such as torrefied biomass. Located at TU Wien, the ARA reactor quantifies the reactivity and conversion behavior of alternative reducing agents (ARAs) under BF-like conditions [2].

Computational fluid dynamics (CFD) has proven to be an invaluable tool for enhancing our understanding of phenomena inside existing equipment or industrial plants [3–5]. A detailed CFD simulation of the ARA reactor allows gaining a deeper understanding of the internal reactor heat transfer and flow fields as well as tracking the particles through the reaction zone.

The combination of experiments and CFD simulations allows for both empirical validation and theoretical exploration, leading to a better understanding of ARA conversion. By incorporating experimental data into a developed

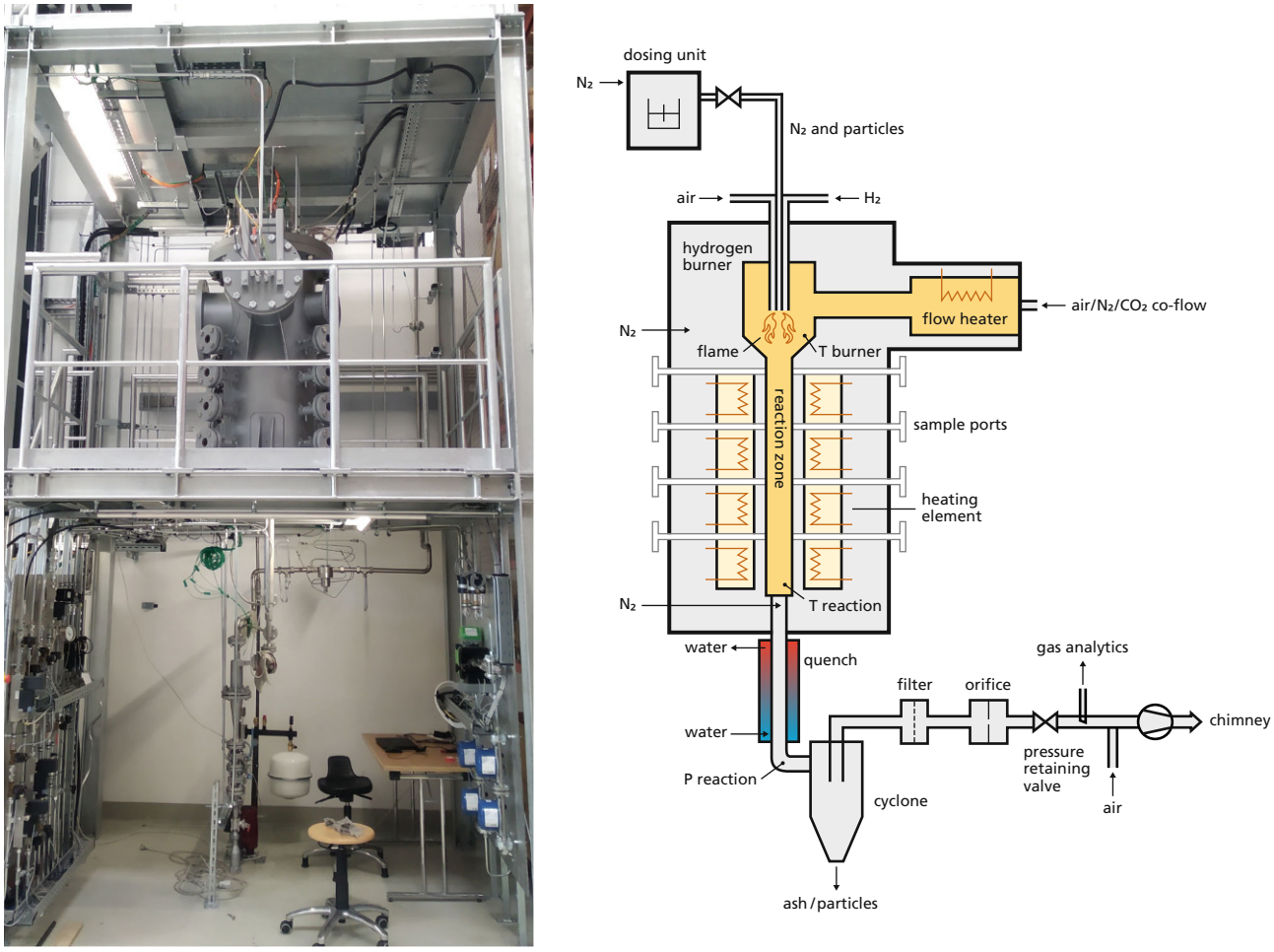

Fig. 1: Image of the ARA reactor setup located at TU Wien (left) and schematic view of the ARA reactor (right)

CFD model, we can refine predictions, explore different scenarios, and identify trends that would otherwise be difficult to detect. This combined approach leads to a more comprehensive understanding of the reactivity and conversion behavior of PC blends and other ARAs under BF-like conditions, enabling better-informed decision-making regarding the application of different ARAs in the BF. In this article, we present the one-of-a-kind ARA reactor, designed to serve as a test reactor for standardized testing of PC and other ARAs. Plant commissioning was completed successfully and intensive trial campaigns using different PC grades are currently planned. Furthermore, we present the developed CFD simulation tool that describes the internal flow, heat transfer, and reactions inside the ARA reactor. Finally, we compare the simulation results to an experiment conducted using the ARA reactor, proving the validity of the developed simulation tool.

2. ARA Reactor—Experimental Setup

The ARA reactor of K1-MET located at and operated with TU Wien is an entrained pressurized flow reactor designed to reproduce BF raceway conditions. Figure 1 shows the ARA reactor setup.

In previous studies, blast temperature, heating rate, pressure, residence time, and relative gas-particle velocity were identified as key design parameters for a test reactor to resemble BF conditions [6]. Typical BF raceway conditions are summarized and compared to the ARA reactor's design parameters in Table 1.

The ARA reactor consists of seven key components: A dosing unit, a flow heater, a hydrogen burner, one reaction zone, a quench, a cyclone, and a filter. Figure 1 sketches the ARA reactor and its main components.

TABLE 1
Comparison of raceway conditions to operation conditions of the new test rig [6, 7]

	Temperature (°C)	Heating rate ($K s^{-1}$)	Pressure (kPa)	Gas velocity (m s^{-1})	Particle velocity (m s^{-1})	Residence time (ms)	O_2 content (vol%)
Raceway	1200–2300	10^4–10^6	200–500	200	20	200–100	~e27
Test rig	<1800	10^4–10^6	100–800	4–30	1–2	50–200	<25

TABLE 2
Overview of reaction conditions

Pressure (kPa)	Flow heater (°C)	Heating elements (°C)	Co-flow (N m^3 h^{-1})	Cooling air (N m^3 h^{-1})	Burnout (–)
310	1050	1400	40	2.5	0.901

The dosing unit provides a constant particle flow of about 1–2 g/min into the reactor. The flow heater pre-heats the main co-flow stream to up to 1100 °C before the hydrogen burner provides a high-temperature zone and radiative heat flux for the particle heat-up. The particles are injected through the middle of the burner lance, which is cooled by the combustion air. The burner directs the co-flow and particle stream into the electrically heated reaction zone. The reaction zone consists of a 0.9 m long ceramic tube. Sixteen sample ports are distributed around the tube on four levels for extracting probes or granting optical access. During the commissioning phase, these ports were not yet accessible. In the water-cooled quench, the off-gas is diluted with nitrogen and cooled down to stop the reaction. Solid residuals down to approximately 1 µm are separated from the off-gas in the cyclone, while a filter removes smaller fractions. An orifice measures the flow rate before the pressure regulation valve. Afterwards, an online gas analyzer and a gas chromatograph (GC) determine species concentrations, and the off-gas leaves the system.

The reaction conditions of the experimental run, which is compared with the CFD simulation, are depicted in Table 2. The experiments were conducted without the hydrogen burner. An airflow through the burner lance cools it during the experiments to prevent the injected particles from clogging the lance. The burnout was derived using the ash tracer method [8]. The ash mass fractions were determined using thermogravimetric analysis (TGA) according to DIN 51734. Bituminous coal with 32% volatile matter and a carbon content of 73% was injected into the reactor.

3. CFD Simulation

Limited temperature measurements in pressurized entrained flow reactors hinder the validation of temperature and velocity uniformity. Consequently, computational fluid dynamics (CFD) plays a crucial role in understanding reactor behavior.

The developed CFD model simulates coal combustion in a multiphase gas-solid environment using OpenFOAM's *reactingFoam* solver. The model incorporates detailed combustion chemistry, turbulence, and radiation modeling. The numerical framework follows an Eulerian-Lagrangian approach, with the gas phase treated as Eulerian and coal particles tracked using Lagrangian equations. The gas-phase flow is governed by the Navier-Stokes equations for mass, momentum, energy, and species transport. The solid-phase particles follow Newton's second law, accounting for convective and radiative heat exchange, drying, devolatilization, and char oxidation. Combustion kinetics include volatile release, homogeneous gas-phase reactions, and heterogeneous char oxidation.

Accurate thermo-physical properties are essential for reliable simulations. Thermal conductivity, typically measured at 1013.25 mbar, is influenced by conduction, convection, and radiation [9]. The developed CFD model assumes pressure-independent thermal conductivity for the particles. The GRI3.0 mechanism, which is described in [10] in detail, was used to ensure accurate fluid transport properties and homogeneous reactions inside the reactor.

The reactor operates in a transitional flow regime, with a Reynolds number between 4000 and 5500. While predominantly laminar, localized turbulence arises from coal injection and buoyancy effects. The k-ω-SST turbulence model (shear stress transport model, one of the most common approaches to model turbulence with reasonable computational cost) is employed for an enhanced accuracy in transitional flow regions. Thermal radiation is incorporated using the discrete ordinates method, assuming gray mean absorption for gas-phase radiation. The Reynolds-averaged Navier-Stokes (RANS) equations are solved using the semi-implicit method for pressure linked equations (SIMPLE). The co-flow enters above the coal injection point at ambient conditions, and nitrogen is used to inject coal particles and quench reactions in the sample probe. All particles and fluid exit through the probe.

The boundary conditions applied in the simulation were chosen to fit the experimental reactions conditions given in Table 2. The input char properties are summarized in Table 3. The computational mesh consists of $1.5 \cdot 10^6$ hexahedral cells, ensuring an adequate resolution to capture key flow features in this complex model.

The simulations were carried out using a two step approach: i) a steady reactor state was obtained without the presence of coal particles first, ii) particles were tracked through the reactor on the previously obtained reactor state. This approach is possible because of the low coal mass flow rate. Simulations were assumed to be in steady-state when the residuals were below 10^{-3} for the pressure and below 10^{-4} for the remaining variables.

Figure 2 displays the simulation domain. For the CFD simulations of the ARA reactor, only the reaction zone,

TABLE 3
Char properties

Particle size	15–200 µm
Density	858 kg m^{-3}
Specific heat capacity	1268 J kg^{-1} K^{-1}
Thermal conductivity	0.04 W m^{-1} K^{-1}
Emissivity	1
Moisture fraction	0.011
Volatile fraction	0.337
Carbon mass fraction (db)	0.9
Ash mass fraction (db)	0.1

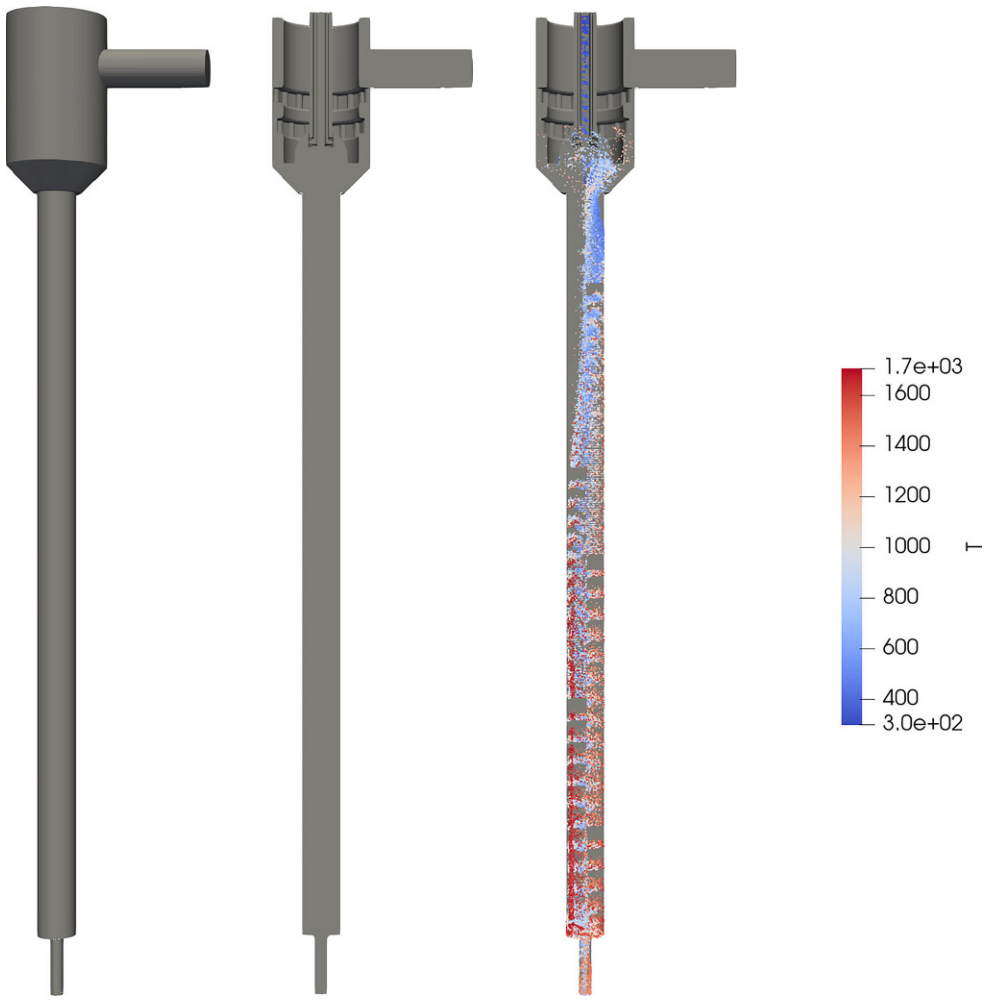

Fig. 2: Shown are (from left to right) the outside of the simulated geometry, a cut through the center, and the particle trajectories with the particle temperature. Particles and co-flow are injected from the top, as well as from the side into the burner unit. The particles then traverse the full reaction zone

which consists of the burner at the top, the ceramic pipe, and the quench, is modeled. Particles and N_2 are injected at the top and are combined with the hot air coming from the flow heater on the right side (see also Fig. 1).

In Figure 3, the individual particles can be seen exiting the particle lance at various velocities. Figure 4 shows the average reaction conditions the particles face along their trajectories through the reactor. The simulation results contain information about the mean residence time of the particles inside the reactor (~e0.31 s), as well as the actual reaction conditions inside the reactor as the particles travel through it. Furthermore, particle heating rates and thermochemical states can also be extracted from the simulation data.

The residence time of the test rig given in Table 1 (50–200 ms) is the gas residence time without particle injection. The particle residence time is expected to be longer due to drag and turbulence making the simulated average particle residence time of 0.31 s reasonable. The average particle burnout in the simulations is 0.87 and is therefore in good agreement with the experimentally determined burnout of 0.901 (see table Table 2).

The CFD simulations also let us estimate whether the gas temperature and the average particle temperature reach the desired values inside the reaction zone. With gas and particle temperatures of up to 1600 K, the simulations show that the reactor reaches the desired reaction conditions.

4. Conclusion

In this contribution, we present the experimental ARA reactor and its digital CFD model. The presented ARA reactor recreates BF conditions and allows investigating the suitability of different ARAs for the BF. To show the validity of the developed digital model of the ARA reactor, the simulations were compared with a performed experiment. The temperatures, residence time of the particles and the calculated burnout suggest a good agreement of the simulation and the experiment.

The presented results clearly indicate the potential of CFD-aided experiments. Complex flow structures, which are present in most experimental equipment, cannot be adequately described by residence times based on the plug flow assumption. Furthermore, the CFD model confirms that the desired high particle heating rate in the order of ($10^5\,K\,s^{-1}$) can be achieved with the ARA reactor design.

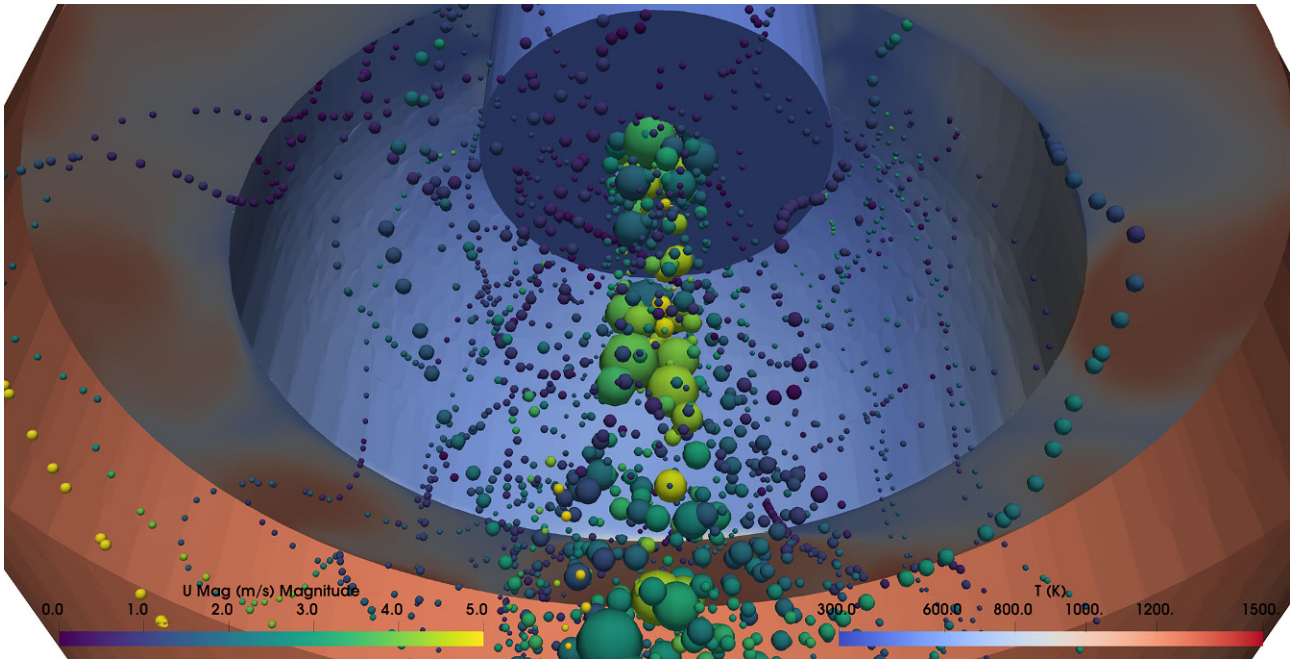

Fig. 3: Simulation results: Particles exiting the lance at the top of the reactor

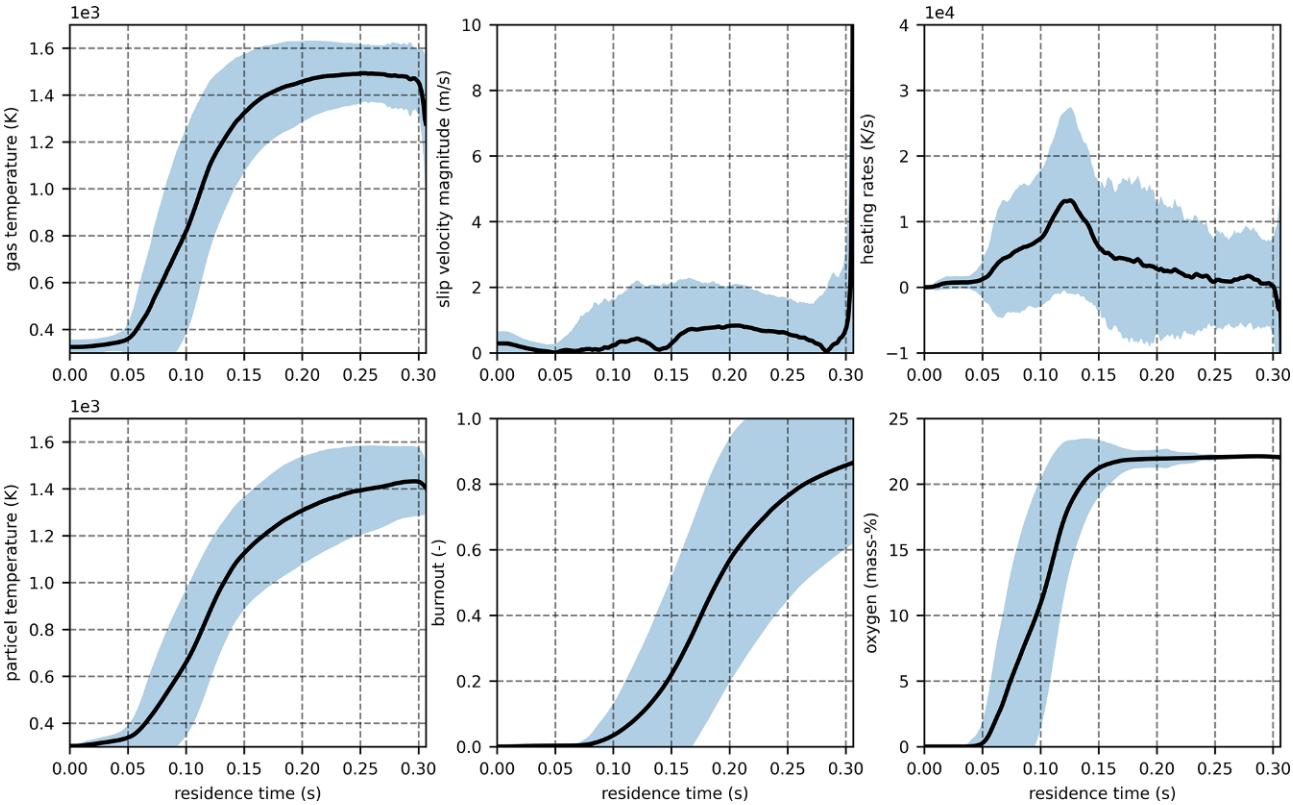

Fig. 4: Simulation results: Carrier gas temperature, slip velocity, particle heating rates, internal particle temperature, burnout, and carrier gas oxygen concentration that are encountered by particles inside the ARA reactor during the CFD simulations. The solid line is the mean value, while the shaded area shows the standard deviation calculated over 1000 particles

The development of the ARA reactor and the accompanying CFD simulation tool represent a significant step forward in understanding the conversion processes of ARAs in BF conditions. The digital model provides additional insights to the experimental processes and enables sophisticated optimization of experimental conditions. Furthermore, spatially resolved velocity, temperature, and species distributions can be obtained from CFD simulations, which can improve the experimental evaluation routines.

Acknowledgements. The authors acknowledge the funding support of K1-MET GmbH, whose research program is supported by COMET (Competence Center for Excellent Technologies), the Austrian program for competence centers. COMET is funded by the Austrian ministries BMK and BMDW, the provinces of Upper Austria, Tyrol, and Styria, and the Styrian Business Promotion Agency (SFG). The authors acknowledge TU Wien Bibliothek for financial support through its Open Access Funding Programme.

Apart from funding, the project activities are financed by the industrial partners Primetals Technologies Austria, voestalpine Stahl, voestalpine Stahl Donawitz, RHI Magnesita, and the scientific partner Technische Universität Wien.

Funding. Open access funding provided by TU Wien (TUW).

References

1. Ng, K.W., Giroux, L., Todoschuk, T.: Value-in-use of biocarbon fuel for direct injection in blast furnace ironmaking. Ironmak. Steelmak. **45**(5), 406–411 (2018). https://doi.org/10.1080/03019233.2018.1457837
2. Nanz, T., Bösenhofer, M., Rieger, J., Stocker, H., Feilmayr, C., Harasek, M.: Evaluating auxiliary reducing agents in a test rig under raceway conditions. In: AISTech, The Iron and Steel Technology Conference And Exposition (2024) https://doi.org/10.33313/388/024
3. Raghavan, V., Whitney, S.E., Ebmeier, R.J., Padhye, N.V., Nelson, M., Viljoen, H.J., Gogos, G.: Thermal analysis of the vortex tube based thermocycler for fast dna amplification: Experimental and two-dimensional numerical results. Rev. Sci. Instrum. **77**(9), 94301 (2006). https://pubs.aip.org/aip/rsi/article-pdf/doi/10.1063/1.2338283/13476439/094301_1_online.pdf https://doi.org/10.1063/1.2338283
4. Lemaire, R., Menanteau, S.: Development and numerical/experimental characterization of a lab-scale flat flame reactor allowing the analysis of pulverized solid fuel devolatilization and oxidation at high heating rates. Rev. Sci. Instrum. **87**(1), 15104 (2016). https://pubs.aip.org/aip/rsi/article-pdf/doi/10.1063/1.4938542/13912211/015104_1_online.pdf https://doi.org/10.1063/1.4938542
5. Bösenhofer, M., Hecht, E., Shaddix, C.R., König, B., Rieger, J., Harasek, M.: Computational fluid dynamics analysis of char conversion in sandia's pressurized entrained flow reactor. Rev. Sci. Instrum. **91**(7), 74103 (2020). https://doi.org/10.1063/5.0005733
6. Bösenhofer, M., Wartha, E.-M., Jordan, C., Feilmayr, C., Stocker, H., Hauzenberger, F., Rieger, J., Tjaden, S., Walk, A., Harasek, M.: Suitability of pulverised coal testing facilities for blast furnace applications. Ironmak. Steelmak. **47**(5), 574–585 (2020). https://doi.org/10.1080/03019233.2019.1565152
7. Harasek, M., Maier, C., Jordan, C., Bösenhofer, M., Feilmayr, C.: Investigation of Alternative Reducing Agent Conversion in the Raceway Cavity of Blast Furnaces by Numerical Simulation. In: AISTech, The Iron and Steel Technology Conference And Exposition (2016)
8. Gat, N., Cohen, L.M., Witte, A.B., Denison, R.M.: Ash loss and the "seeded-tracer" technique for the determination of mass balance in rapid heating coal pyrolysis experiments. Combust Flame **57**(3), 255–263 (1984). Accessed 2025-02-14 https://doi.org/10.1016/0010-2180(84)90045-2
9. Litovsky, E., Shapiro, M., Shavit, A.: Gas pressure and temperature dependences of thermal conductivity of porous ceramic materials: Part 2, refractories and ceramics with porosity exceeding 30. J. Am. Ceram. Soc. **79**(5), 1366–1376 (1996)
10. Smith, G.P., Golden, D.M., Frenklach, M., Moriarty, N.W., Eiteneer, B., Goldenberg, M., Bowman, C.T., Hanson, R.K., Song Jr., S., , W.C.G., Lissianski, V.V., Qin, Z.: GRI-Mech 3.0. Available at (1999). http://www.me.berkeley.edu/gri_mech/, Accessed 14 Apr 2025